Submitted to:
The European Physical Journal A

COSMIC AND SUBATOMIC PHYSICS REPORT
LUIP 9802
AUGUST 1998
ISRN LUNFD6/NFFK-7157-SE+32P
ISSN 0348-9329

An experimental study of ^{1,2,3}H, ^{3,4,6}He, ^{6,7,8,9}Li, ^{7,9,10,11}Be and ^{10,11,12}B isotope production from interactions of 14A and 32AMeV ^{14}N with ^{112,124}Sn

A.Fokin[1], O.V.Lozhkin[2], V.Bellini[3], M.Berg[1], A.Bogdanov[2], J.P.Bondorf[4], A.Budzanowski[5], L.Carlén[1], C.Conelli[3], M.Cronquist[6], B.Czech[5], R.Elmér[1], G.Ericsson[7], R.Ghetti[1], M.Guttormsen[8], J.Helgesson[1], D.Idier[4], K.Ieki[9], B.Jakobsson[1], J.Julien[10],A.Kuznetsov[2], V.Lyapin[2], G.Løvhøiden[8], F.Merchez[11], I.Mishustin[4], T.Motobayashi[9], Y.Murin[1], J.Mårtensson[1], B.Norén[1], J.Nyberg[7], K.Nybø[13], A.Oskarsson[1], G.Riera[3], A.Siwek[1], Ö.Skeppstedt[6], I.Skwirczynska[5], L.Sperduto[3], C.Sutera[3], T.F.Thorsteinsen[13], L.Westerberg[7], H.J.Whitlow[1], M.Zubkov[2]

(CHIC collaboration)

and A.Larionov[3]

[1] *Department of Physics, Lund University, Box 118, S-22100 Lund, Sweden*
[2] *V.G.Khlopin Radium Inst., 197022 St.Petersburg, Russia*
[3] *INFN, Sez di Catania, I-95129 Catania, Italy*
[4] *Niels Bohr Inst., DK-2100 Copenhagen, Denmark*
[5] *Henryk Niewodniczanski Inst. of Nucl.Phys., PL-31-342 Krakow, Poland*
[6] *Chalmers Inst. of Technology, S-41296 Gothenburg, Sweden*
[7] *The Swedberg Lab., S-75121 Uppsala, Sweden*
[8] *Dept. of Physics, Oslo Univ., N-0315 Oslo, Norway*
[9] *Rikkyo Univ., Tokyo 171, Japan*
[10] *CEN Saclay, F-91191 Gif-sur-yvette, France*
[11] *ISN Grenoble, F-38026 Grenoble, France*
[12] *Inst. for Nucl. Studies, PL-00-681, Warsaw, Poland*
[13] *Dept. of Physics, Univ. of Bergen, N-5000 Bergen, Norway*

Cosmic and Subatomic Physics
University of Lund
Box 118
S-221 00 Lund, Sweden

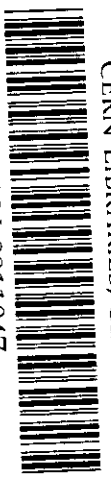

An experimental study of ^{1,2,3}H, ^{3,4,6}He, ^{6,7,8,9}Li, ^{7,9,10,11}Be and ^{10,11,12}B isotope production from interactions of 14A and 32AMeV ^{14}N with ^{112,124}Sn

A.Fokin[1], O.V.Lozhkin[2], V.Bellini[3], M.Berg[1], A.Bogdanov[2], J.P.Bondorf[4], A.Budzanowski[5], L.Carlén[1], C.Conelli[3], M.Cronquist[6], B.Czech[5], R.Elmér[1], G.Ericsson[7], R.Ghetti[1], M.Guttormsen[8], J.Helgesson[1], D.Idier[4], K.Ieki[9], B.Jakobsson[1], J.Julien[10],A.Kuznetsov[2], V.Lyapin[2], G.Løvhøiden[8], F.Merchez[11], I.Mishustin[4], T.Motobayashi[9], Y.Murin[1], J.Mårtensson[1], B.Norén[1], J.Nyberg[7], K.Nybø[13], A.Oskarsson[1], G.Riera[3], A.Siwek[1], Ö.Skeppstedt[6], I.Skwirczynska[5], L.Sperduto[3], C.Sutera[3], T.F.Thorsteinsen[13], L.Westerberg[7], H.J.Whitlow[1], M.Zubkov[2]

(CHIC collaboration)

and A.Larionov[3]

[1]*Department of Physics, Lund University, Box 118, S-22100 Lund, Sweden*
[2]*V.G.Khlopin Radium Inst., 197022 St.Petersburg, Russia*
[3]*INFN, Sez di Catania, I-95129 Catania, Italy*
[4]*Niels Bohr Inst., DK-2100 Copenhagen, Denmark*
[5]*Henryk Niewodniczanski Inst. of Nucl.Phys., PL-31-342 Krakow, Poland*
[6]*Chalmers Inst. of Technology, S-41296 Gothenburg, Sweden*
[7]*The Swedberg Lab., S-75121 Uppsala, Sweden*
[8]*Dept. of Physics, Oslo Univ., N-0315 Oslo, Norway*
[9]*Rikkyo Univ., Tokyo 171, Japan*
[10]*CEN Saclay, F-91191 Gif-sur-yvette, France*
[11]*ISN Grenoble, F-38026 Grenoble, France*
[12]*Inst. for Nucl. Studies, PL-00-681, Warsaw, Poland*
[13]*Dept. of Physics, Univ. of Bergen, N-5000 Bergen, Norway*

Abstract

Experimental results on light particle and intermediate mass fragment formation in interactions of ^{14}N (E = 14A and 32A MeV) with ^{112,124}Sn are presented. Mass identefication for all fragments with Z$\leq$5 and energies $\geq$1 MeV/nucleon has been obtained and their double differential cross sections have been measured in the angular interval 24^0-155^0. Standard parameters like temperatures and velocities have been determined for two Maxwellian sources defined from the invariant cross section contours in the parallel-transverse momentum plane. The ratios of the fragment yields from reactions with ^{112}Sn and ^{124}Sn targets are studied. Quantum molecular dynamics calculations with a local Pauli potential have been applied to describe the light particle and fragment production.

1 Introduction

The phenomena of nuclear fragmentation and multifragmentation in interactions of high energy particles and heavy ions with atomic nuclei are important to study in connection with the attempts to describe the equation of state of baryonic matter [1]. The lack of understanding of the formation of highly excited nuclear matter and its decay as well as of how clusters are formed is, however, still hampering this description

Experimental and theoretical investigations during the last decades show multiple production of intermediate mass fragments (IMF, $3 \leq Z_f \leq 20$) in different kinds of reactions [2, 3]. Fundamental characteristics of baryonic matter such as temperature, compressibility, clusterization and instabilities at low density can be studied in this multifragment emission.

Though the first indication of a liquid-gas phase transition in nuclear matter has emerged from experiments with the ALADIN detector [4], more results are required for a solid evidence. The first results confirm qualitatively the prediction from the statistical multifragmentation model [5], which states that a nuclear phase transition does occur.

The experiments, described in this paper aim at investigating the intermediate mass fragment production in reactions induced by relatively low energy (14 and 32A MeV) heavy ions in isotope enriched target nuclei (^{112,124}Sn). Heavy ion reactions in this energy domain are of a complex transitional nature [6]. The excited compound nucleus formation (complete fusion) and its decay via sequential evaporation or fission changes to incomplete fusion, deep inelastic and at higher energies also participant/spectator reactions. In the ^{14}N+^{112,124}Sn reactions studied here, the IMF emission comes from sources which are similar in size, excitation energy, Coulomb barrier, etc. but differ in isospin and also in the IMF binding energy. The "isotopic effect", i.e. the systematic evaluation of the yield of a specific fragment from sources which differ in the number of neutrons (N) but not in charge (Z) has been studied earlier at higher beam energies [7]. This gives a possibility to evaluate the temperature of the decaying system in a parameter-free way [8]. In the first study of fragmentation at much lower energies, (this experiment) we found evidence for an intermediate source, the decay of which can be described by equipartition statistics [8].

2 Details of the experiment

The data have been obtained in two experiments at the Gustav Werner cyclotron at The Svedberg laboratory, Uppsala, Sweden. Beams of ^{14}N ions with energies of 14A and 32A MeV and intensities 5-20 nA bombarded ^{112}Sn and ^{124}Sn self-supporting target foils with thicknesses of $\approx$1mg/cm^2. The isotopic purity of the target was 79.9% for ^{112}Sn and 95.3% for ^{124}Sn. The beam current was measured with a Faraday cup. Three multidetector Si-telescopes were placed inside a vacuum chamber and one monitoring telescope outside a 50 μm stainless steel window. Two telescopes consisted of six Si-detectors (the last one acting as veto detector) with thicknesses from 14 up to 3500 μm which allowed to register fragments with energies from $\approx$0.7 MeV/nucleon up to $\approx$50 MeV/nucleon. The other two telescopes were intended for measurements of high energy particles and consisted of a combination of a 300μm Si detector and one CsI(Tl) scintillator with a thickness of 26 or 40 mm. This sets the upper energy limit for protons to 80 or 120 MeV. The setup actually registered all fragments up to their kinematical limits, so the energy limits were actually set by statistics. Detailed telescope parameters are listed in Table 1. The energy calibration of the Si-detectors was performed with point-like ^{241}Am alpha sources (5.49 MeV), placed on the frame of each detector. In addition the back-bending points of the dE-E matrices, which correspond to maximal energy delivered to the E-detectors, were used. The uncertainty of the energy with this method was estimated as $\lesssim$ 4%. The energy calibration of the CsI detectors was performed by placing the calibrated Si-detectors in front of them during bombardment. The angular range covered in the experiments was 24^0 to 155^0 (lab. system). The systematic errors in the absolute cross sections were $\approx$20%. Actually additional measurements at 62^0 and 90^0 degrees have been performed with telescopes exchanged in order to verify the absolute cross sections. These measurements show the same spectral shapes and absolute cross sections (within 10%) which confirms the correctness of the evaluation of the systematic errors.

3 General experimental results

The double differential cross sections of ^{1,2,3}H, ^{3,4,6}He, ^{6,7,8,9}Li, ^{7,9,10,11}Be, ^{10,11,12}B from ^{14}N+^{112,124}Sn reactions at 14A and 32A Mev at 8 angles were measured. These data allow systematic studies of emission sources with

particular emphasize on the importance of their isospin. Fig. 1 shows spectra of H,He,Li,Be and B isotopes measured at 25^0, 48.5^0, 62^0, 70^0, 90^0, 104^0, 131.5^0 and 155^0 from ^{14}N+^{124}Sn reaction at 32AMeV. Fig. 2 shows some spectra measured at 70^0. The following general features of the spectra are similar to what is observed in reactions of high energy protons with ^{112,124}Sn targets [7]:

- The anisotropy of the particle emission significantly increases with particle energy.
- The shape of the fragment spectra is the same for the two Sn targets but the absolute cross section depends on N_t/Z_t and N_f/Z_f ratios (t stands for target and f for fragment). As pointed out earlier [8] this depends on both the difference in separation energy of fragments and in Coulomb barrier.
- An important feature of the fragment energy distribution is the production of secondary particles below the Coulomb barrier. This indicates a significantly reduced Coulomb potential in the decaying system. Emission of sub-barrier fragments has been discussed in [9, 10] both in reactions induced by high energy and intermediate energy particles. This effect can possibly be explained by partial loss of charge in the target nucleus at the pre-equilibrium stage of the reaction or by fast decay (multifragmentation). Expansion of the source will also decrease the effective Coulomb barrier for the fragmentation process. The effect of expansion are discussed in [11].
- The shape of the double differential cross sections for protons and fragments (Fig.1) can not be described in terms of one single Maxwell-Boltzmann like moving source in equilibrium.

4 Source analysis

Invariant, $1/p\ d^2\sigma/dEd\Omega$, cross section contours in the parallel-perpendicular momentum plane exhibit the existence of at least two well separated sources. Fig.3 shows some examples of such contour plots. One slow source (SS), moving with a velocity < 0.02 c (less than the CM velocity) and one intermediate source (IS), moving with about half the nucleon-nucleon (NN) CM velocity

are recognized. In some cases a third fast source (FS), associated with the projectile, is indicated, but it is normally not observed because of the experimental angular cutoff at 24^0. The slow source has actually a minimum in the cross section at its center typical for Coulomb repulsion, while this is not observed at all for the IS. The SS is generally believed to be associated with deep inelastic reactions or incomplete fusion for more central reactions. The intermediate source is associated with pre-equilibrium emission and the fast source is associated with projectile residue evaporation in peripheral collisions. The simplest description of the spectra is a sum of two or three Galilei transformed Maxwell-Boltzmann like sources

$$\frac{d^2\sigma}{dE'd\Omega'} = const \cdot (E' - V_f) \cdot e^{-\frac{E'-V_f}{T}} \tag{1}$$

where

$$E' = E + E_0 - 2\sqrt{E \cdot E_0} \cdot cos(\Theta) \tag{2}$$

for surface emission or

$$\frac{d^2\sigma}{dE'd\Omega'} = const \cdot \sqrt{(E' - V_f)} \cdot e^{-\frac{E'-V_f}{T}} \tag{3}$$

for volume emission. E and E' are kinetic energies of the fragment in the lab and CM systems respectively, Θ is the emission angle in the laboratory system, E_0 is the energy of the emitting source in the lab. system and V_f is the effective Coulomb barrier. Spectra are transformed to the laboratory system as,

$$\frac{d^2\sigma}{dEd\Omega} = \sqrt{\frac{E}{E'}} \cdot \frac{d^2\sigma}{dE'd\Omega'} \tag{4}$$

A proper introduction of the smearing of the Coulomb barrier modifies (1),

$$\frac{d^2\sigma}{dE'd\Omega'} = const \cdot \int_{k-D}^{k+D} (E' - k \cdot V_f) \cdot e^{-\frac{E'-k\cdot V_f}{T}} dk \tag{5}$$

Where k and D are the reduction factor and the width of the smearing. In practice (1) can be simplified to,

$$\frac{d^2\sigma}{dE'd\Omega'} = const \cdot E' \cdot e^{-\frac{E'}{T}} \tag{6}$$

for the intermediate source. In order to fit the inclusive spectra with a sum of two Maxwellians, some of the parameters must be fixed or at least given initial values. The following procedure has been used.

- Velocities of the moving sources were estimated from the $p_{\parallel} - p_{\perp}$ plots. Thereby the velocity of the SS was fixed at 0.017c for 32A MeV and 0.010c for 14A MeV reactions for all fragments. It should be stressed that the small velocity at 14A MeV is in disagreement with the linear momentum systematics [12] in incomplete fusion reactions. This shows the fact that at 14AMeV there is a strong mixture between incomplete fusion and other, peripheral, reactions where the target-like source gets a very small velocity. The velocity of the IS is different for different fragments and it was e.g. set to 0.12c for ^{6}Li fragments from the 32A MeV N+^{124}Sn reactions.

- Since practically only emission from the slow source contributes at the very backward angles, the temperature of this source, and its Coulomb barrier were determined from these spectra.

- A separate fit is performed to inclusive energy spectra for each angle (Figs.4,5). It is required that $\chi^2/d.o.f$ <1 to accept the fit. The angular dependence for the slow and intermediate source is then obtained by integrating the cross sections (5) and/or (6) over all particle energies (Fig.6,7). The angular dependence may be described as,

$$\frac{d\sigma}{d\Omega} = a_i \cdot e^{-b_i \Theta} \tag{7}$$

The SS emits particles rather isotropically in the lab system, while the IS has the strong forward anisotropy.

- The total cross section, σ, of particle emission is taken as a sum of two cross sections, σ_1 and σ_2, representing the slow and intermediate sources.

All parameters determined by the procedure described above is presented in tables 2-5. Besides total and partial cross sections, the tables give extracted temperatures, which fall in the region 2.5-4.5 MeV for the slow source

and 12-15 MeV for the intermediate one. These temperatures remain approximately the same for all types of emitted particles which suggests that all particles are of the same origin.

The results show that the total elemental cross section (fragments with the same Z) are larger for the light target isotope. This agrees with the results in reference [13] and demonstrates the "isotopic effect" for fragmentation [4, 10].

The temperature of the slow equilibrized source with isotropic CM emission falls in the region of 4-6 MeV. This is very close to the "chemical" temperature, which can be estimated from the relative yields of excited fragments [15], from the "isotopic effect" [8] or from combined ratios of light fragments [16]. As shown in [8], the chemical temperature of the excited source, estimated from the isotopic effect in ^{14}N(32A MeV) +^{112,124}Sn reactions is 4.94±0.35 MeV for He - Be fragments.

In the next chapter we combine a dynamic model for ^{14}N+Sn interactions with statistical deexcitation through particle emission.

5 Theoretical interpretation

5.1 Overview

Statistical descriptions of fragmentation are based on the assumption that the final products occupy the whole available phase-space uniformly [17, 19], and they have proven to be useful in predicting a variety of observables in intermediate energy heavy ion reactions. Such descriptions explain in particular the large IMF multiplicity. However such approaches neglect all dynamics of the reaction and they can therefore not be expected to answer any question about how emission sources are created. Instead various hybrid models have been created, where a dynamical prescription is added to the statistical decay.

With microscopic models one can investigate nuclear reactions without making any specific assumptions about the reaction mechanism. There are many kinds of microscopic theories, such as time dependent Hartree-Fock (TDHF) [20] , which describes the mean field, the Vlasov, the Vlasov Uehling-Uhlenbeck (VUU) or Boltzmann Uehling-Uhlenbeck (BUU) [21, 22] equations, that incorporate both the mean field interaction and two-body collisions and the cascade model [23] which stresses two-body collisions.

The BUU model [22] is often combined with sequential evaporation [24] from the remaining residue. As shown in [6], one can get a good description of invariant cross section contour diagrams for nucleons if a mean field potential, corresponding to a "soft" equation of state,

$$V(\rho) = -365\frac{\rho}{\rho_0} + 303\left(\frac{\rho}{\rho_0}\right)^{7/6} MeV, \tag{8}$$

is chosen and if a strongly reduced Coulomb field of the residual nucleus is taken into account. Such calculations lead to fusion-like reactions at small impact parameters and to deep inelastic reactions at large impact parameters and therefore two separate sources (slow and fast) of fragment production appears. The BUU model is however basically a one-body model, which cannot describe the formation process of complex fragments, although experimentally, contour diagrams for complex particles are observed which are quite similar to those of protons.

5.2 PQMD calculations

Quantum molecular dynamics (QMD) [25], or nuclear molecular dynamics (NMD) [26] are models developed to investigate both reaction dynamics and fragment formation. The semiclassical nature of the standard QMD does not make it applicable for low energy heavy ion reactions (below 50A MeV), but several modified versions of the original model have appeared. Antisymmetrized molecular dynamics (AMD) [27] and Fermionic molecular dynamics (FMD) [28] treat the many-body nature of the antisymmetrized Fermionic system with numerical methods, while Pauli molecular dynamics (PQMD) [29] and extended molecular dynamics (EQMD) [30] models include the Pauli potential part in the Hamiltonian. In PQMD the total energy of the "free" Fermi gas system is given by,

$$E_{tot} = E_{kin} + E_{Pauli} = \sum_i \frac{\mathbf{p}_i^2}{2m} + \frac{1}{2}\sum_{i\neq j} V_{Pauli}^0 \left[\frac{\hbar}{q_0 p_0}\right] \exp\left[-\frac{r_{ij}^2}{2q_0^2} - \frac{p_{ij}^2}{2p_0^2}\right] \delta\tau_i\tau_j\delta\sigma_i\sigma_j \tag{9}$$

where τ_i and σ_i denote the spin and isospin of nucleon i. Furthermore, the Hamiltonian is written as,

$$H = E_{kin} + E_{Pauli} + V_{Coulomb} + V_{Yukawa} + V_{Skyrme} \tag{10}$$

and the nucleons are represented by gaussian wave packets of the form,

$$f_i(\mathbf{r}_i, \mathbf{p}_i, t) = \frac{1}{(\pi\hbar)^3} \exp\left\{ -\frac{[\mathbf{r}_i - \mathbf{r}_{i0}(t)]^2}{2L} - [\mathbf{p}_i - \mathbf{p}_{i0}(t)]^2 \frac{2L}{\hbar^2} \right\}, \qquad (11)$$

propagating according to classical equations of motions for their centroids ($\mathbf{r}_{i0}$ and $\mathbf{p}_{i0}$). The stochastic nature of the collision and Pauli blocking in the final state is also incorporated. The inclusion of the Pauli potential gives this model a well defined Fermionic ground state, which is very important for low energy reactions (below 50A MeV) Then it becomes possible to provide excitation energies to the emitted fragments and therefore to describe secondary decay properly. In order to show the importance of the Pauli potential we calculated the fragment mass distributions from the ^{14}N(32A MeV)+^{124}Sn reaction in both the NMD and PQMD approach (Fig. 8). The NMD ground state of the incident nuclei, as well as of the emitted fragments, are not well defined and this leads to further emission of nucleons which gives a significant mass shift of the target and projectile-like residues. Consequently, NMD overestimates the yields of light particles.

The statistical multifragmentation model (SMM) is introduced for deexcitation of fragments and residues, remaining after the dynamical stage of the PQMD calculations. Such deexcitation is very important for a correct description of the reaction mechanism and leads to significant changes in the mass distribution of reaction products, as shown in Fig. 8.

Fig. 9 shows double differential cross sections of protons and deuterons calculated in the frame of the PQMD+SMM approach. Good agreement with data is observed. While PQMD correctly describes production of high energy particles, the SMM is essential for description of low energy particles especially at backward angles. The calculated $p_{\|} - p_{\perp}$ contour plot for protons from the ^{14}N(32A MeV)+^{124}Sn reaction (Fig. 10) confirms the existence of two well separated sources of particle emission with positions and relative strengths in agreement with experimental observations (Fig. 3). In order to understand the nature of these sources the emitted protons were separated into direct PQMD products and decay products from the target or projectile-like part. Fig. 11 shows the energy spectrum of protons from ^{14}N(32AMeV) + ^{124}Sn reaction and its composition. The slow source with (slope) temperature of about 4MeV is formed by the decay products of the target residual. The corresponding fast source has an apparent (slope) temperature of 17 MeV which can be translated to a proper source tempera-

ture (5.5-6.0 MeV) after transformation to the rest system of the projectile. These particles build up the high-energy tail of the spectrum. The intermediate source is represented by the directly emitted protons. The (slope) temperature of this source is about 12 MeV, which corresponds well to the experimentally observed temperature. It should be emphasized that particles in this region of the energy spectra are products of dynamic processes and no specific "thermal" source is connected with it. Instead, the observed temperature should be regarded as "kinetic". This differs significantly from the "chemical" temperatures connected with particle emission from equilibrated thermal sources.

Fig. 9 shows that the model correctly describes production of secondary particles below the Coulomb barrier. The reduction of the Coulomb barrier in the PQMD model is due to the partial loss of charge in the equilibrated target residue at the dynamic stage of the reaction and by the expansion of this source after preequilibrium emission has taken place.

The time-scale of the reaction was also investigated in the frame of the PQMD+SMM approach. Fig. 12 shows how the total multiplicity varies with time. The projectile and target nuclei form a "compound" binary system which exists for about 50-75 fm/c and after that time the fast dynamic emission of particles during about 10-20 fm/c takes place. The system becomes fully equilibrated after about 300 fm/c. Then the SMM "afterburner" should be switched on. This process will increase the charged particle multiplicity further.

6 Conclusion

The emission of light particles and intermediate mass fragments at angles $\geq 24^0$ in N+Sn,Au collisions at 14A and 32A MeV exhibits clearly two sources, an equilibrized target- or incomplete fusion-like source with velocity 0.01-0.02c and temperature 2.5-5 MeV and a non-equilibrium, intermediate source of dynamical origin with velocity close to the NN CM and "kinetic" temperature 12-15 MeV. A combination of a dynamic model and a statistical model, here the PQMD+SMM combination, for decay of both residues and excited fragments reproduces data well. Comparing the emission from ^{14}N+^{112}Sn and ^{14}N+^{124}Sn reactions show little difference in the spectral form but substantial difference in the individual yields. These differences are related to different separation energies, different isospin and different Coulomb

barriers.

We wish to thank the Swedish Natural Science Research Council for its financial support and the staff of the Gustaf Werner cyclotron at the Svedberg Laboratory for its technical support.

7 Figure Captions

Figure 1. Double differential cross sections of fragments emitted in ^{14}N+^{124}Sn reactions at 32A MeV. a) for H and He fragments, b) for Li and Be fragments and c) for B fragments. Lab. angles are labelled on the first figure.

Figure 2. Double differential cross sections of H and He fragments emitted at 70^0 in ^{14}N+^{124}Sn reactions at 32A MeV.

Figure 3. Invariant cross section contours in the $p_{\|} - p_{\perp}$plane of p (left) and ^{6}Li (right) fragments emitted in ^{14}N+^{124}Sn reactions at 14A MeV (upper) and 32A MeV (lower). The a.u. numbers correspond to the cross section given in logarithmic scale..

Figure 4. Double differential cross sections for ^{6}Li produced in ^{14}N+^{124}Sn reactions at 32A MeV. Curves show the fit with two Maxwellian distributions (see text).

Figure 5. ^{6}Li emission cross sections in ^{14}N+^{124}Sn reactions at 32A MeV. The curves show the contribution from the slow, the intermediate and the sum of Maxwellian sources (dotted, dashed and solid).

Figure 6. Angular distribution of Li, Be, B fragments from ^{14}N+^{124}Sn at 32AMeV. Points are results of integration over particle energies. Solid curves represent the total cross section as a sum of the intermediate source (dashed) and slow source (dotted).

Figure 7. Angular distributions of H and He fragments from ^{14}N+^{124}Sn reactions at 32A MeV. Curves as in Fig. 6.

Figure 8. Mass distribution of all products emitted in ^{14}N+^{124}Sn reactions at 32A MeV in different molecular dynamics calculations. NMD = Nuclear Molecular Dynamics, PQMD = Quantum Molecular Dynamics with Pauli potential, SMM = Statistical Multifragmentation Model.

Figure 9a. Proton differential cross sections from $^{14}N+^{124}Sn$ interactions at 32AMeV. Circles - experimental data, dotted lines - PQMD calculations, dashed lines - PQMD+SMM calculations.

Figure 9b. Deuteron production from $^{14}N+^{124}Sn$ at 32A MeV. Circles - experimental data, dotted lines - PQMD calculations, dashed lines - PQMD+SMM calculations.

Figure 10. PQMD+SMM calculations of invariant cross section contours (a.u., log. scale) from protons emitted in $^{14}N+^{124}Sn$ reactions at 32A MeV.

Figure 11. Proton energy spectra (a.u.) calculated in the PQMD+SMM approach. The various contributions are shown by the different curves.

Figure 12. The total particle multiplicity as a function of reaction time in $^{14}N+^{124}Sn$ reactions at 32A MeV calculated in the PQMD approach.

8 Tables

Table 1. Parameters of multidetector telescopes

Telescope	Thickness of detectors, μm
Si 1ΔE-5ΔE	14,4+140+800+2500+550
Si 1ΔE-5ΔE	30+150+1000+2000+1000
Si 1ΔE-5ΔE	33,3+375+2175+3400+525
Si 1ΔE-6ΔE	550+1750+2000+2700+3400+3400
Si + CsI(Tl)	800+26000
Si + CsI(Tl)	2000+40000

Table 2. Maxwellian parameters for fragment spectra in ^{14}N(14AMeV)+^{112}Sn and ^{124}Sn reactions

	^{112}Sn		^{124}Sn	
Fragment	k	T_1, MeV	k	T_1, MeV
^{6}Li	0.25	4.28	0.25	4.37
^{7}Li	0.26	4.95	0.27	3.70
^{8}Li	0.27	4.23	0.25	2.50
^{7}Be	0.37	4.32	0.34	2.50
^{9}Be	0.31	4.60	0.35	4.33
^{10}Be	0.31	3.50	0.37	3.65
^{10}B	0.40	4.00		
^{11}B	0.47	4.70		

Table 3. Maxwellian parameters for fragment spectra in ^{14}N(32AMeV)+^{112}Sn and ^{124}Sn reactions

	^{112}Sn			^{124}Sn		
Fragment	k	T_1,MeV	T_2,MeV	k	T_1,MeV	T_2,MeV
^{6}Li	0.28	4.28	13.0	0.28	4.67	12.0
^{7}Li	0.17	5.40	12.0	0.18	4.90	13.2
^{8}Li	0.33	5.40	12.5	0.24	3.54	13.0
^{7}Be	0.38	4.00	14.0	0.30	3.50	15.0
^{9}Be	0.36	5.50	14.0	0.45	4.01	14.0
^{10}Be	0.40	3.60	15.0	0.36	5.20	14.0
^{10}B	0.56	4.13		0.50	3.57	
^{11}B	0.47	6.10		0.45	4.67	

Table 4. Production cross sections (in mb) for secondary particles in ^{14}N(14AMeV)+^{112}Sn (left) and ^{124}Sn (right) reactions

Fragment	σ_1	σ_2	σ_{tot}	σ_1	σ_2	σ_{tot}
^{6}He				1.38	4.41	5.79
^{6}Li	1.75	11.28	13.04	1.12	7.57	8.69
^{7}Li	2.12	11.88	14.01	1.89	13.11	15.00
^{8}Li				1.67	0.97	2.64
^{7}Be	0.36	1.80	2.16	0.15	0.88	1.03
^{9}Be	0.41	2.81	3.22	0.57	3.99	4.56
^{10}Be	0.18	0.75	0.93	0.61	2.95	3.56
^{10}B	0.97	4.02	5.20			
^{11}B	0.54	3.62	4.16			

Table 5. Production cross sections (in mb) for secondary particles in ^{14}N(32AMeV)+^{112}Sn (left) and ^{124}Sn (right) reactions

Fragment	σ_1	σ_2	σ_{tot}	σ_1	σ_2	σ_{tot}
^{1}H	1841.4	1635.2	3476.6			
^{2}H	232.50	604.80	837.20			
^{3}H	216.90	375.20	592.10			
^{3}He	23.74	249.44	273.18			
^{4}He	848.90	1042.40	1891.30			
^{6}He	8.63	16.31	24.99			
^{6}Li	8.15	39.62	47.75	6.30	27.23	33.53
^{7}Li	10.81	44.63	55.43	11.60	45.80	57.40
^{8}Li	5.25	10.27	15.53	0.20	12.34	12.54
^{7}Be	1.90	20.05	21.95	1.06	10.34	11.40
^{9}Be	3.41	11.00	14.41	1.81	12.76	14.57
^{10}Be	0.45	5.29	5.74	1.99	9.33	11.32
^{10}B	2.48	16.40	19.25	1.48	12.17	13.64
^{11}B	3.44	14.35	17.78	1.54	11.93	13.47

References

[1] H.Jagaman, A.Z.Mekjian and L.Zamik, Phys.Rev. C 27, 2782 (1983); D.Bandyopadhyay et al., Nucl. Phys. A 511, 1 (1990); J.E.Finn et al., Phys.Rev.Lett. 49, 1321 (1982); J.Kapusta, Phys.Rev.C 29, 1735 (1984) and references therein.

[2] B.Jakobsson, G.Jönsson, B.Lindkvist and A.Oscarsson, Z.Phyzik A 307, 293 (1982)

[3] C.Ogilvie et al., Phys.Rev.Lett. 67, 1214 (1991)

[4] W.F.J.Mueller,J.Pochodzalla,W.Trautmann et al., GSI, Nachrichten 03-95 (1995)

[5] J.P.Bondorf et al., Nucl.Phys. A 443, 321 (1985); A 448, 753 (1986)

[6] H.Fuchs and K.Mohring, Rep.Prog.Phys. 57, 231 (1994)

[7] V.I.Bogatin at al., Yad.Fizika 19, 32 (1974), Nucl.Phys. A 326, 508 (1979) and Nucl.Phys. A 260, 446 (1976)

[8] V.Avdeichikov et al., Physics Scripta 50, 624 (1994)

[9] Yu.Murin at al., Phys.Rev. C 51 2794 (1995)

[10] Y.Fujimoto and Y. Yamaguchi, Progr.Theor.Phys. 5, 76 (1950); N.A.Perfilov and O.V.Lozhkin, Russian Journal of Experimental and Theoretical Physics 31 913, (1956)

[11] M.D.Zubkov and O.V.Lozhkin, to be published in Nucl.Phys. A

[12] Y.Chan et al., Phys.Rev. C 27, 447 (1983)

[13] J.Brzychczyk, D.S.Bracken and K.Kwiatkowski, Phys.Rev. C 47, 1553 (1993)

[14] V.I.Bogatin et al., Nucl.Phys. A 326, 508 (1979)

[15] Z.Chen et al., Phys. Lett. B 189, 177 (1987); G.Kunde et al., Phys. Lett. B 272, 202 (1991)

[16] S.Albergo et al., Nuovo Cimento A 89, 1 (1985)

[17] D.H.E.Gross, Rep. Prog. Phys. 53, 605 (1990)

[18] D.Hahn and H.Stocker, Nucl. Phys. A 476, 717 (1988)

[19] J.P.Bondorf, R.Donangelo, I.N.Mishustin, C.J.Pethick, H.Schulz and K.Sneppen, Nucl.Phys. A 443, 321 (1985)

[20] J.W.Negele, Rev. Mod. Phys. 54, 913 (1982)

[21] G.F.Bertsch and S.Das Gupta, Phys. Rep. 160, 189 (1998)

[22] W.G.Gong, W.Bauer, C.K.Gelbke and S.Pratt, Phys. Rev. C 43, 781 (1991)

[23] Y.Yariv and Z.Fraenkel, Phys. Rev. C 20, 2227 (1979)

[24] W.A.Friedman and W.G.Lynch, Phys. Rev. C 28, 10 (1983); W.A.Friedman, Phys. Rev. Lett. 60, 189 (1988); Phys. Rev. C 40, 2055 (1989)

[25] J.Aichelin, Phys. Rep. 202, 233 (1991)

[26] J.P.Bondorf, D.Idier and I.Mishustin, Phys.Lett. B359, 261 (1995)

[27] A.Ono, H.Horiuchi, T.Maruyama and A.Ohishi, Prog. Theor. Phys. 87, 1185 (1992)

[28] H.Feldmeier, Nucl. Phys. A 515, 147 (1990)

[29] G.Peilert et al., Phys. Rev. C46 (1992) 1457

[30] T.Maruyama, K.Niita and A.Iw amoto, Phys. Rev.C 53, 297 (1996)

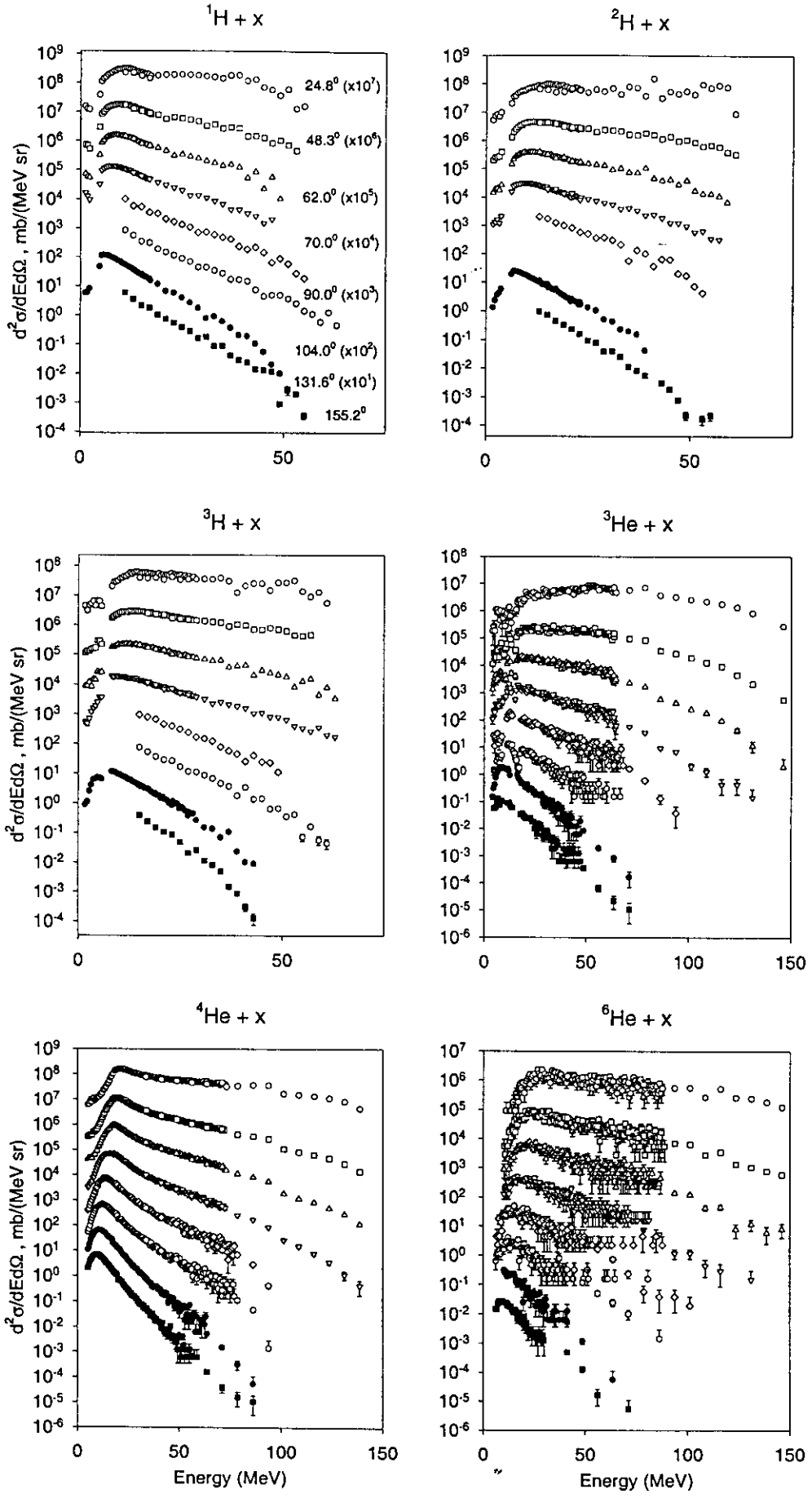
^{1}H + x
^{2}H + x
^{3}H + x
^{3}He + x
^{4}He + x
^{6}He + x
d^{2}σ/dEdΩ , mb/(MeV sr)
24.8^{0} (x10^{7})
48.3^{0} (x10^{6})
62.0^{0} (x10^{5})
70.0^{0} (x10^{4})
90.0^{0} (x10^{3})
104.0^{0} (x10^{2})
131.6^{0} (x10^{1})
155.2^{0}
Energy (MeV)

Fig. 1a

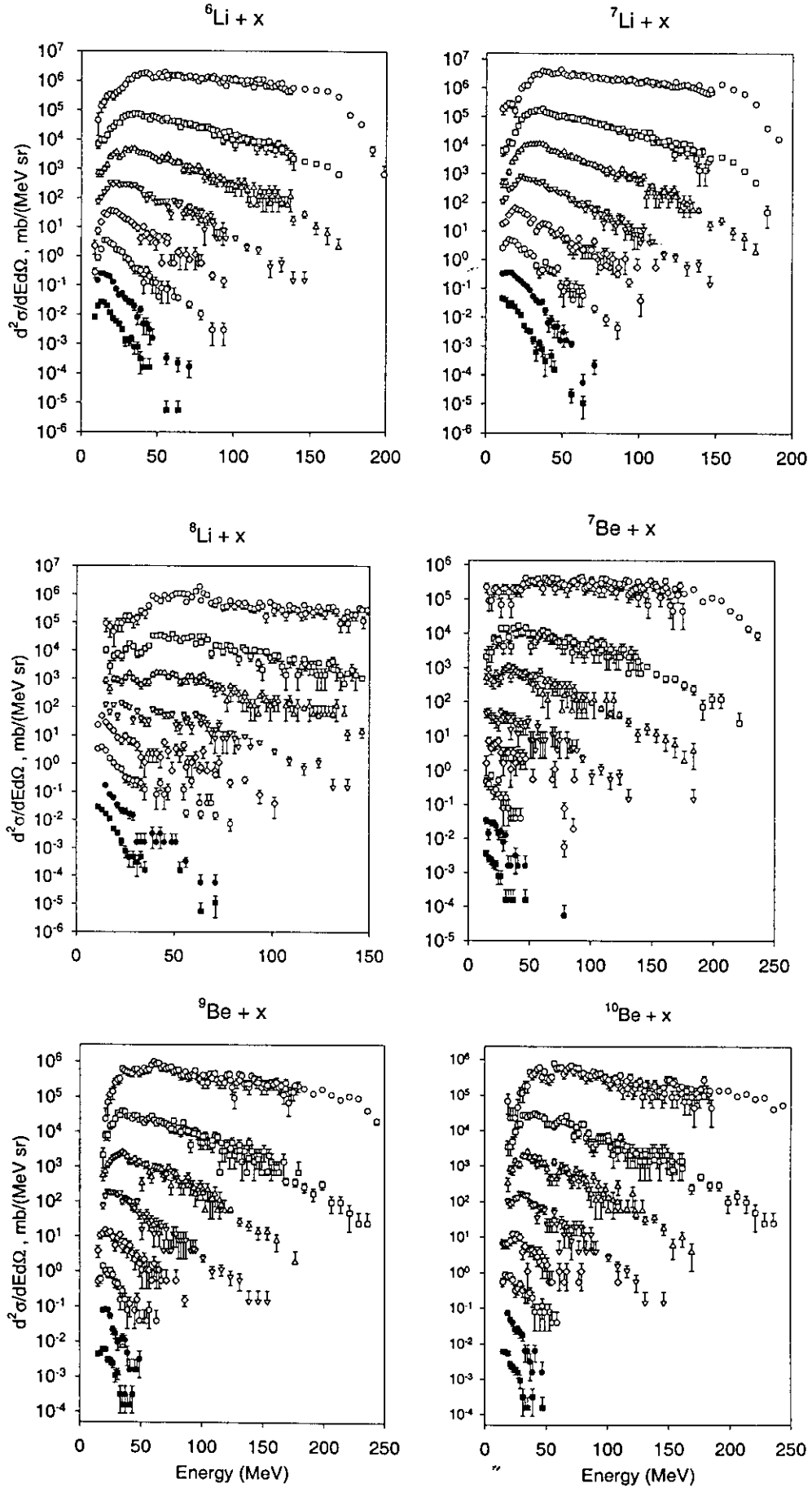

Fig. 1b

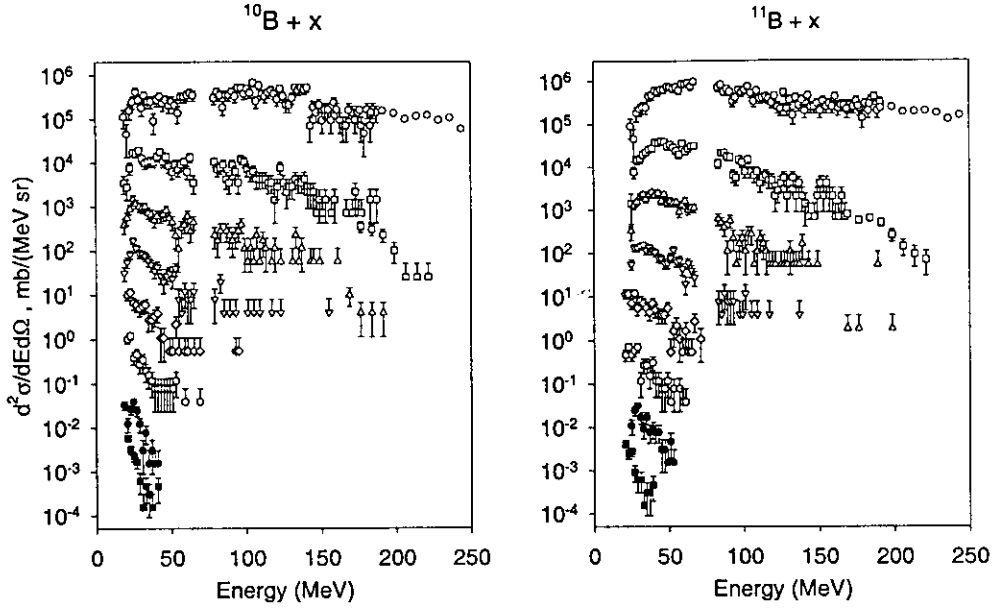

Fig. 1c

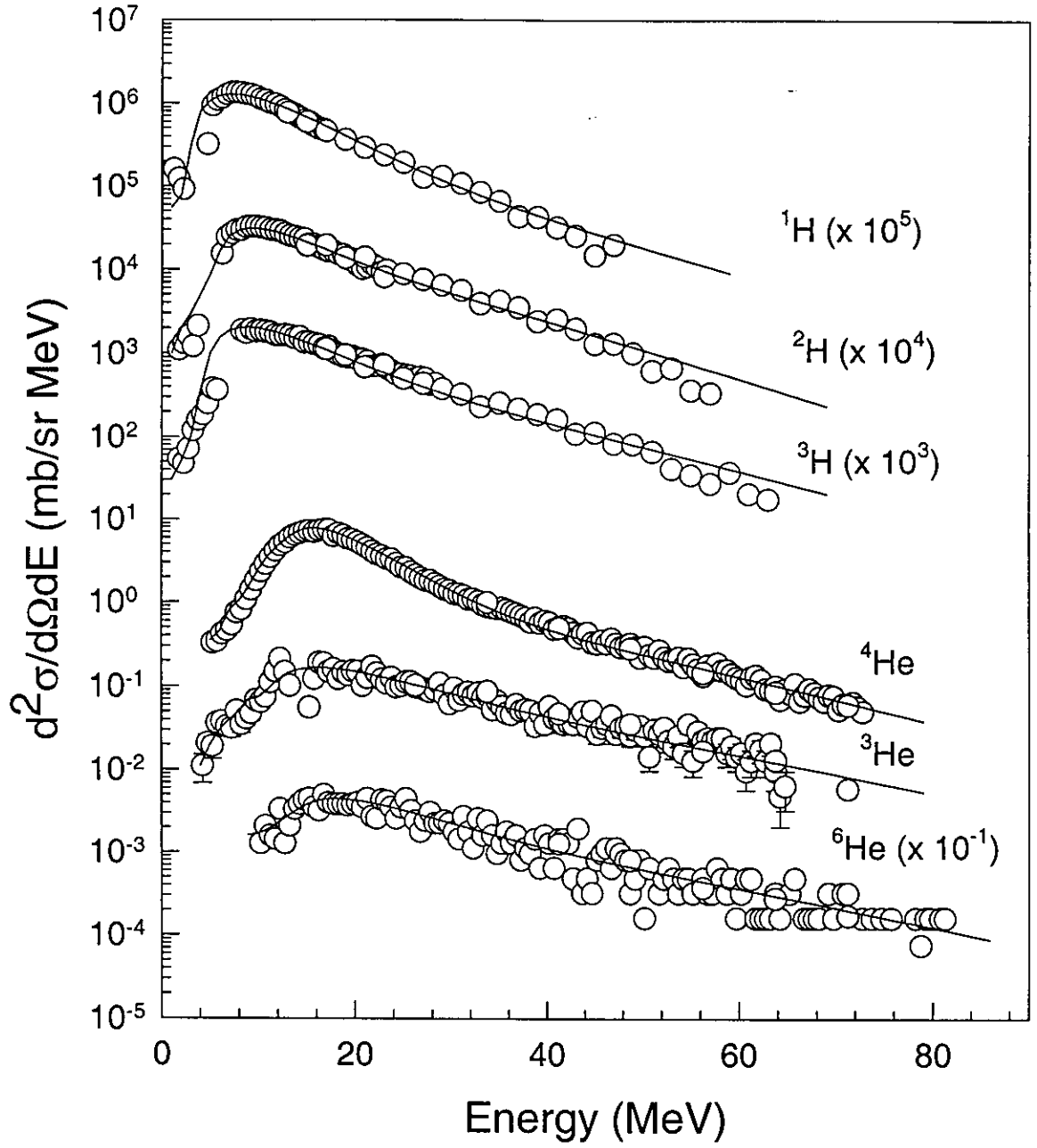
10^7
10^6
10^5
10^4
10^3
10^2
10^1
10^0
10^{-1}
10^{-2}
10^{-3}
10^{-4}
10^{-5}
$d^2\sigma/d\Omega dE$ (mb/sr MeV)
^{1}H (x 10^5)
^{2}H (x 10^4)
^{3}H (x 10^3)
^{4}He
^{3}He
^{6}He (x 10^{-1})
0
20
40
60
80
Energy (MeV)

Fig. 2

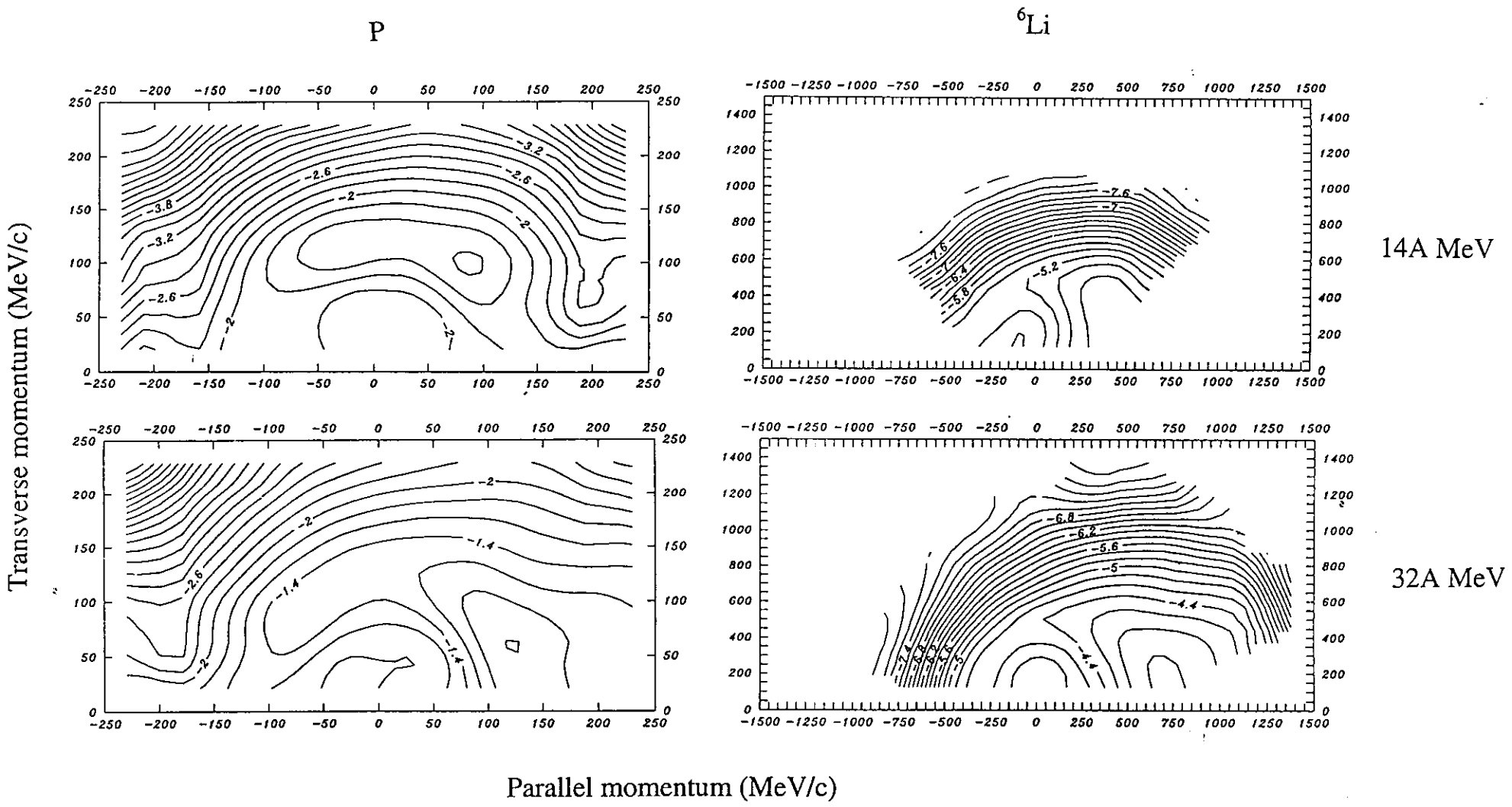
P
^{6}Li
14A MeV
32A MeV
Transverse momentum (MeV/c)
Parallel momentum (MeV/c)

Fig. 3

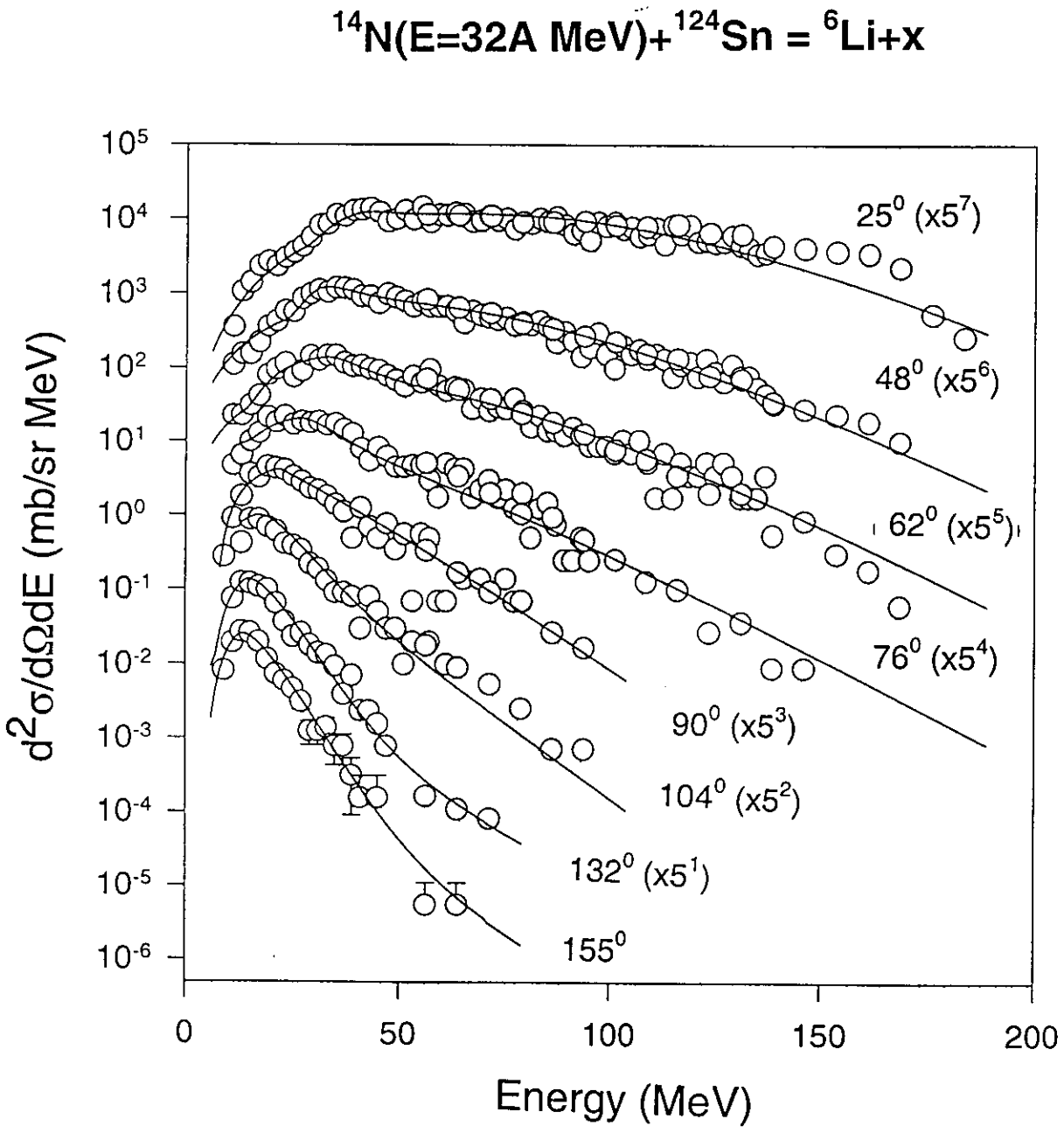
^{14}N(E=32A MeV)+^{124}Sn = ^{6}Li+x
d$^2\sigma$/dΩdE (mb/sr MeV)
Energy (MeV)
25^0 (x5^7)
48^0 (x5^6)
62^0 (x5^5)
76^0 (x5^4)
90^0 (x5^3)
104^0 (x5^2)
132^0 (x5^1)
155^0

Fig. 4

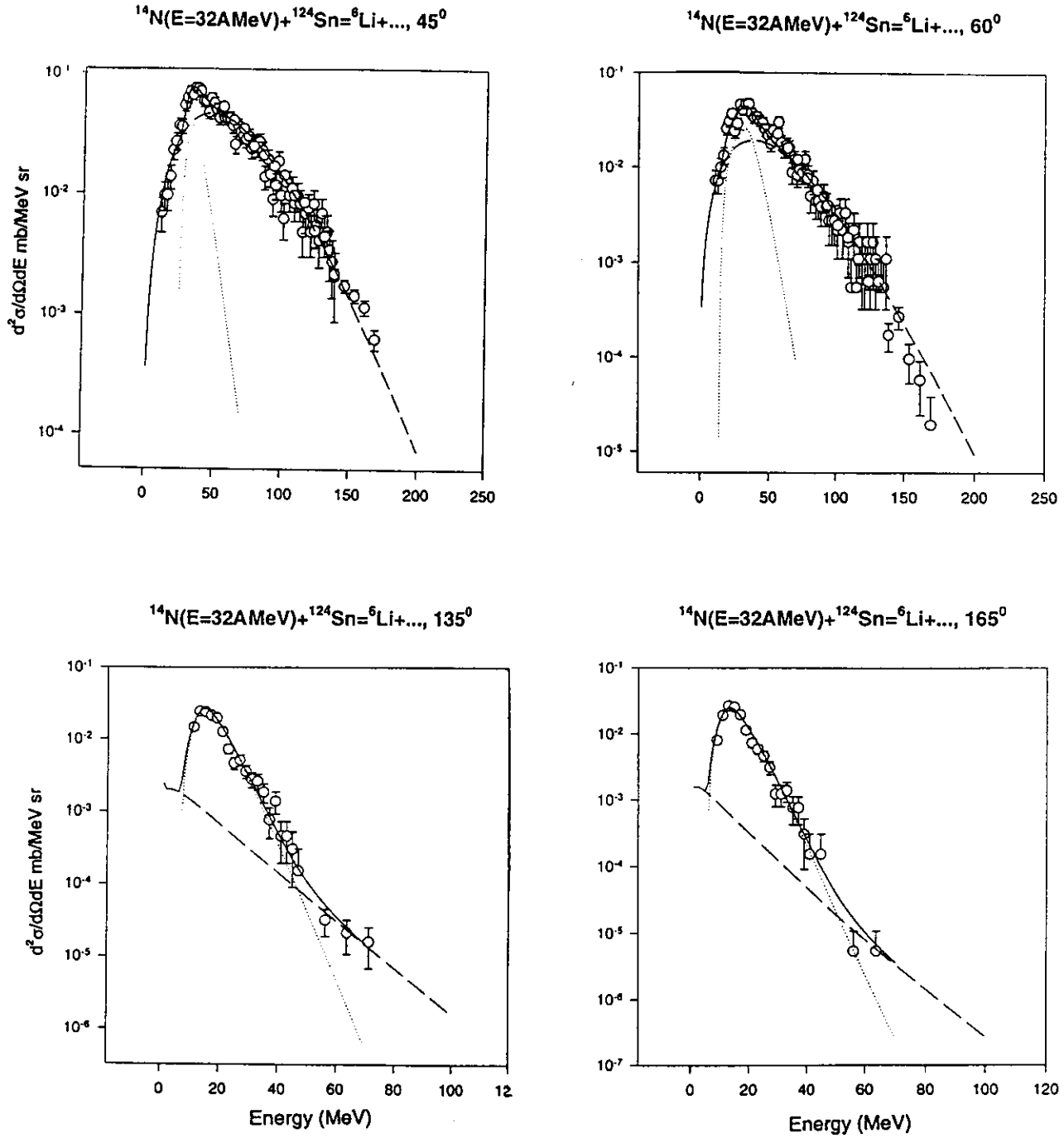
^{14}N(E=32AMeV)+^{124}Sn=^{6}Li+..., 45^{0}
^{14}N(E=32AMeV)+^{124}Sn=^{6}Li+..., 60^{0}
^{14}N(E=32AMeV)+^{124}Sn=^{6}Li+..., 135^{0}
^{14}N(E=32AMeV)+^{124}Sn=^{6}Li+..., 165^{0}
d^{2}σ/dΩdE mb/MeV sr
Energy (MeV)

Fig. 5

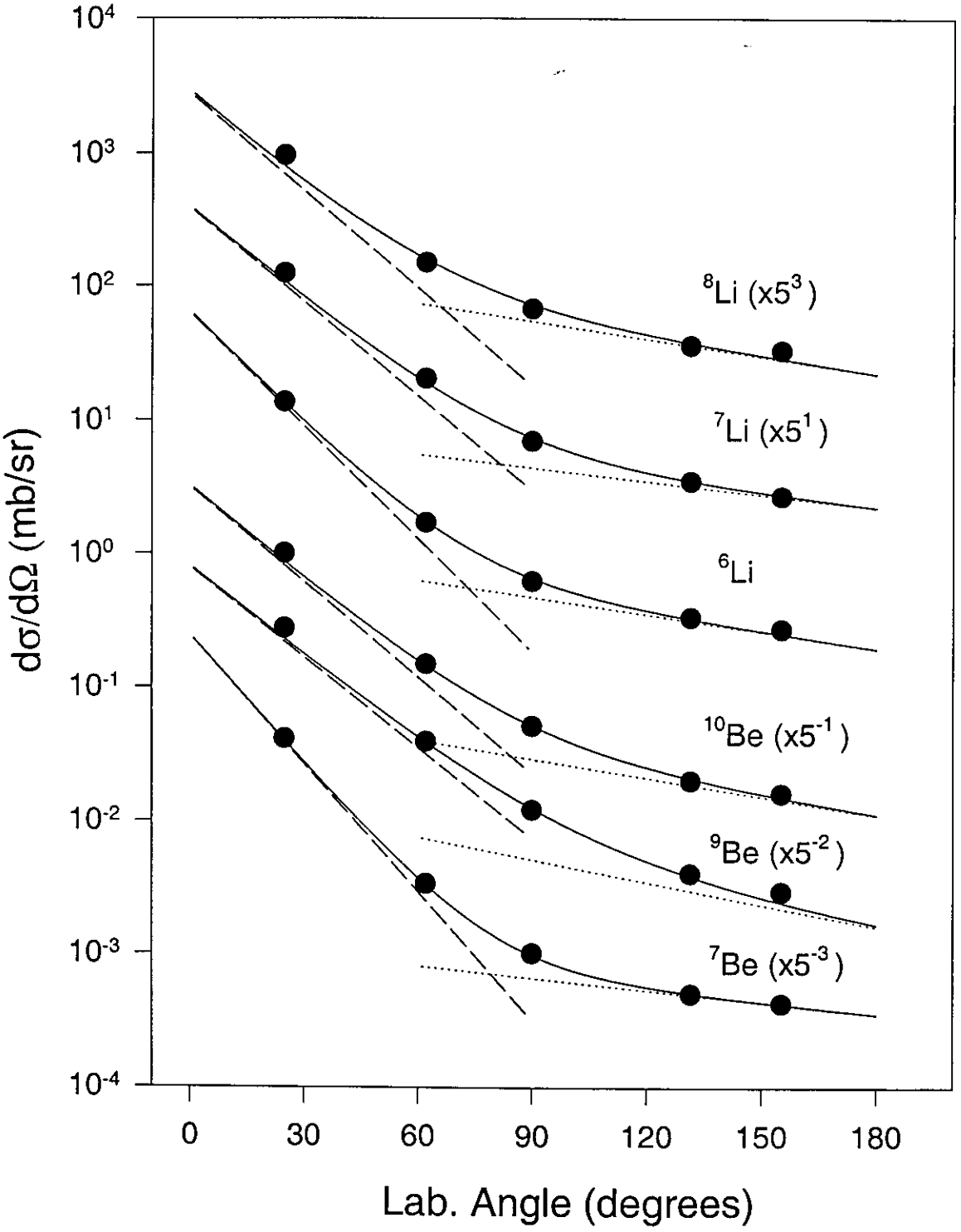
10^4
10^3
10^2
10^1
10^0
10^{-1}
10^{-2}
10^{-3}
10^{-4}
dσ/dΩ (mb/sr)
^{8}Li (x5^3)
^{7}Li (x5^1)
^{6}Li
^{10}Be (x5^{-1})
^{9}Be (x5^{-2})
^{7}Be (x5^{-3})
0
30
60
90
120
150
180
Lab. Angle (degrees)

Fig. 6

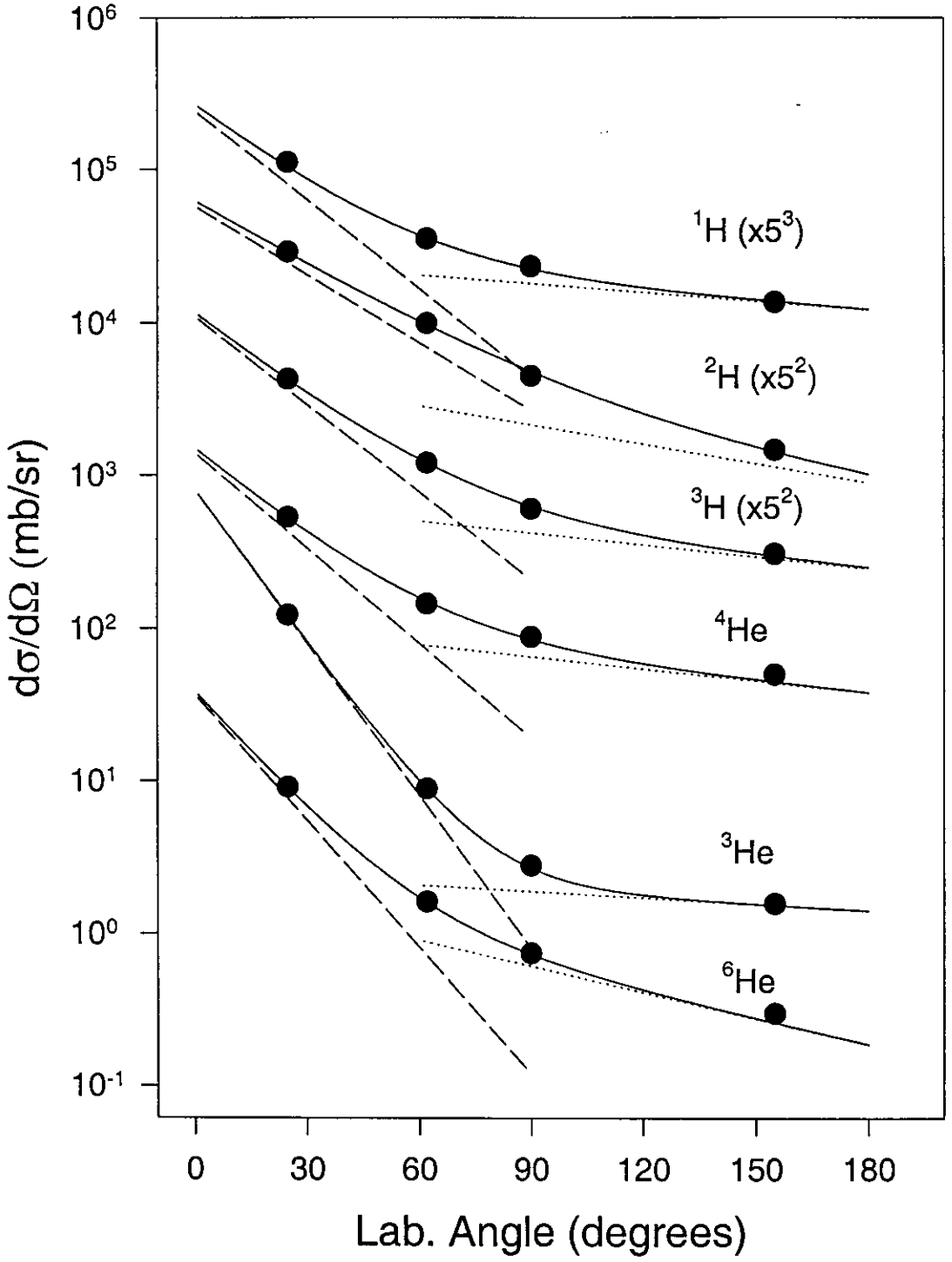
10^6
10^5
10^4
10^3
10^2
10^1
10^0
10^{-1}
dσ/dΩ (mb/sr)
^{1}H (x5^3)
^{2}H (x5^2)
^{3}H (x5^2)
^{4}He
^{3}He
^{6}He
0
30
60
90
120
150
180
Lab. Angle (degrees)

Fig. 7

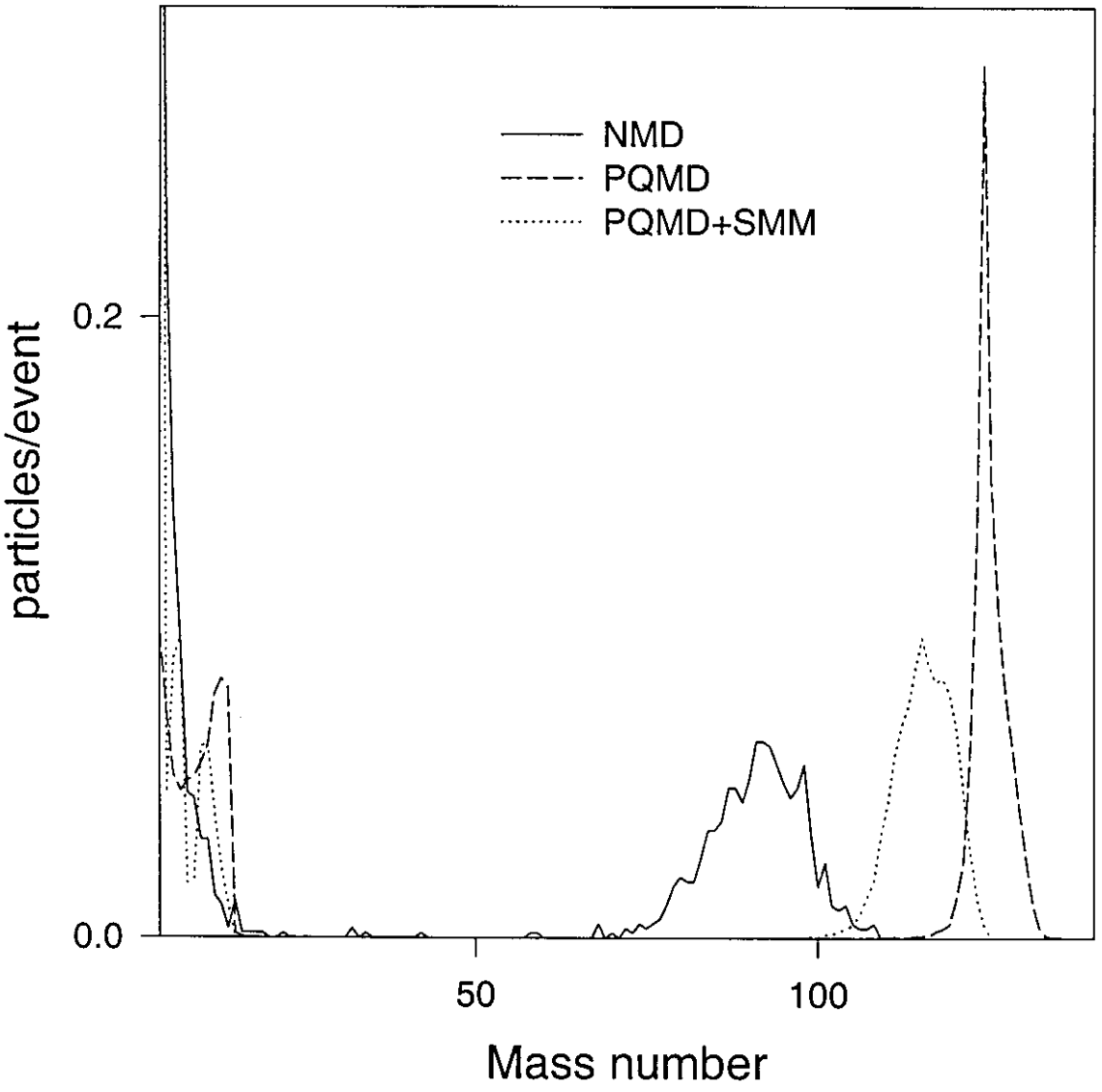

Fig. 8

$^{14}N(32AMeV)+^{124}Sn = p + x$

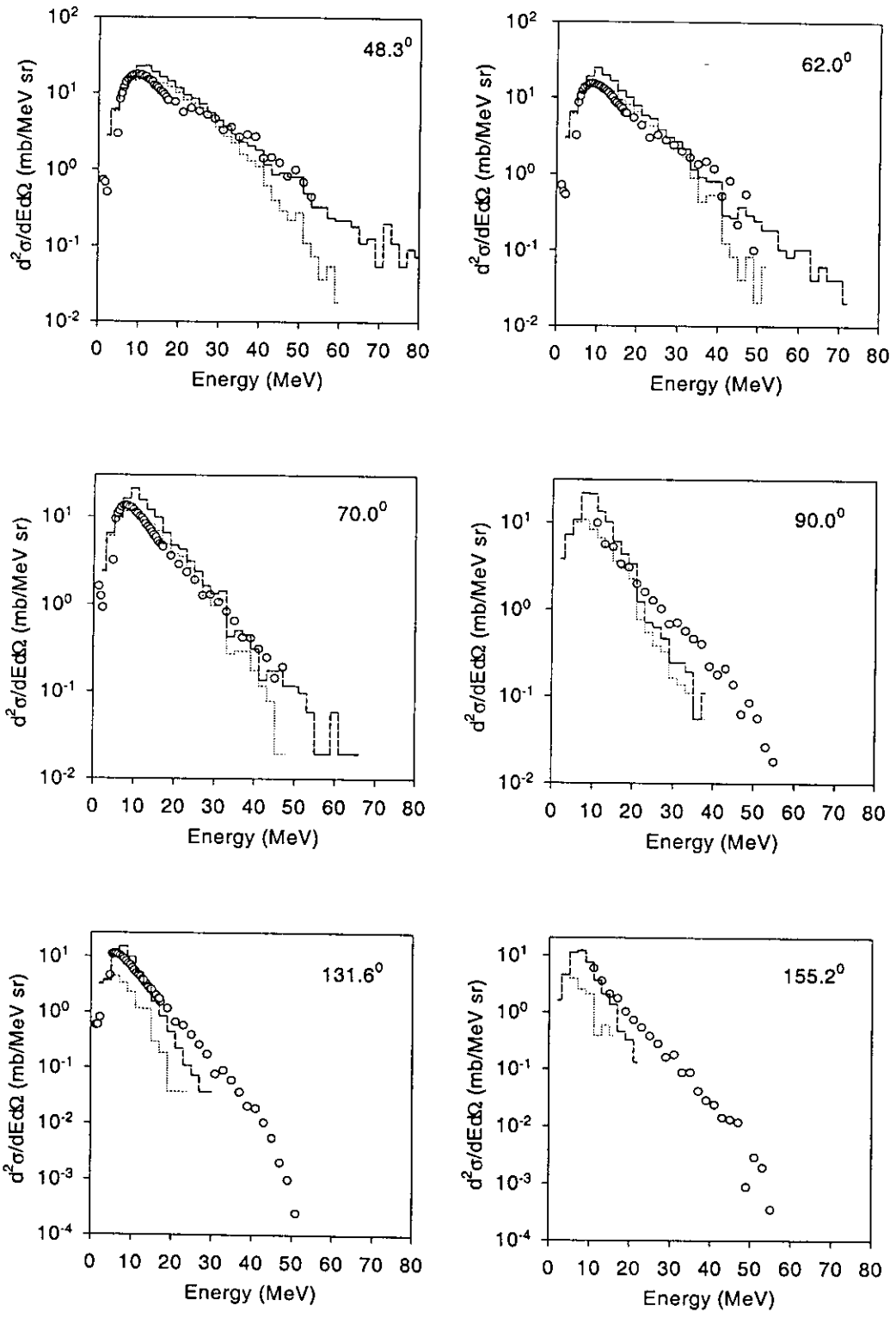

Fig. 9a

$^{14}N(32AMeV)+^{124}Sn = d + x$

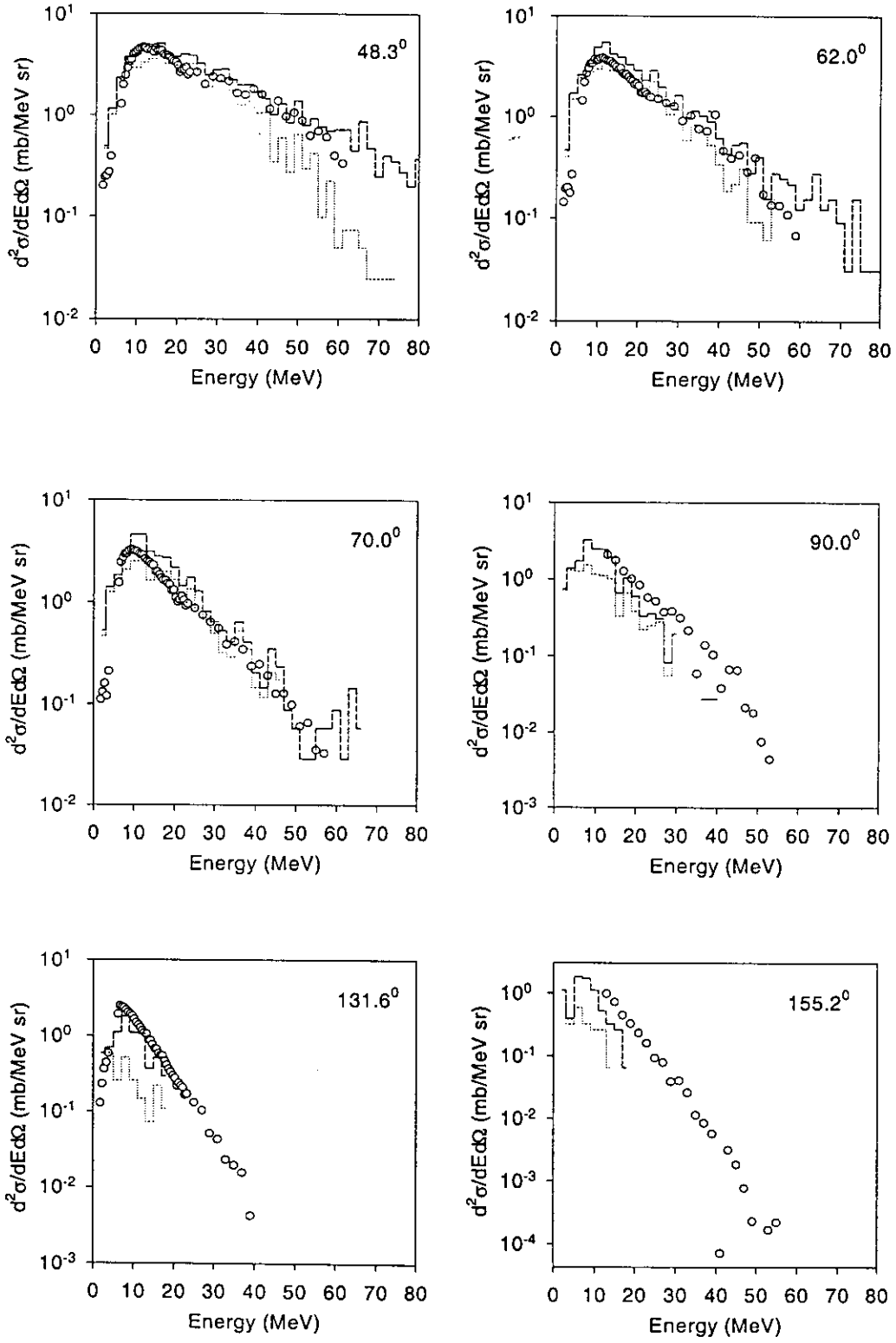

Fig. 9b

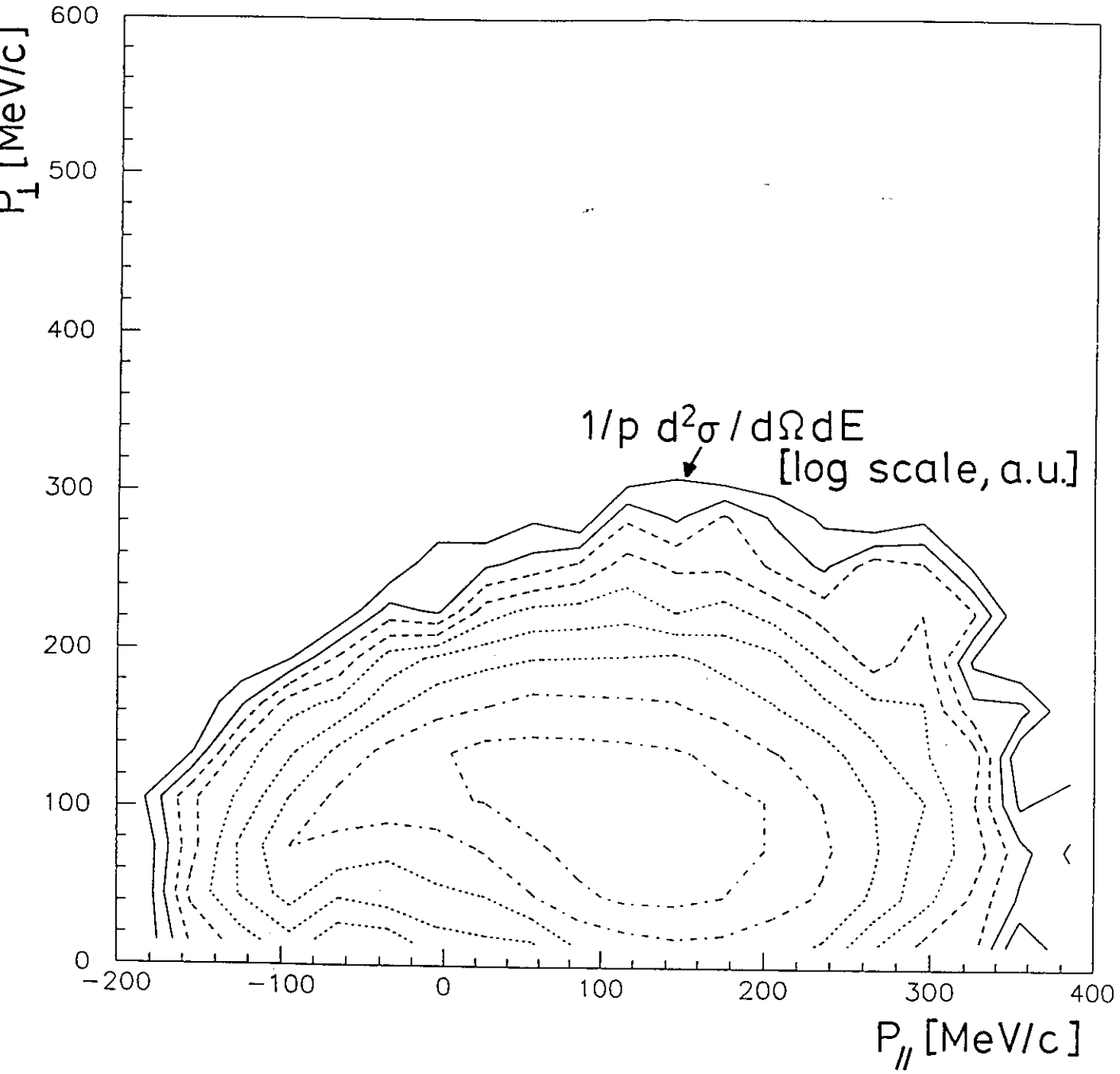
600
500
400
300
200
100
0
$P_\perp$ [MeV/c]
$1/p\ d^2\sigma/d\Omega dE$
[log scale, a.u.]
−200
−100
0
100
200
300
400
$P_{//}$ [MeV/c]

Fig. 10

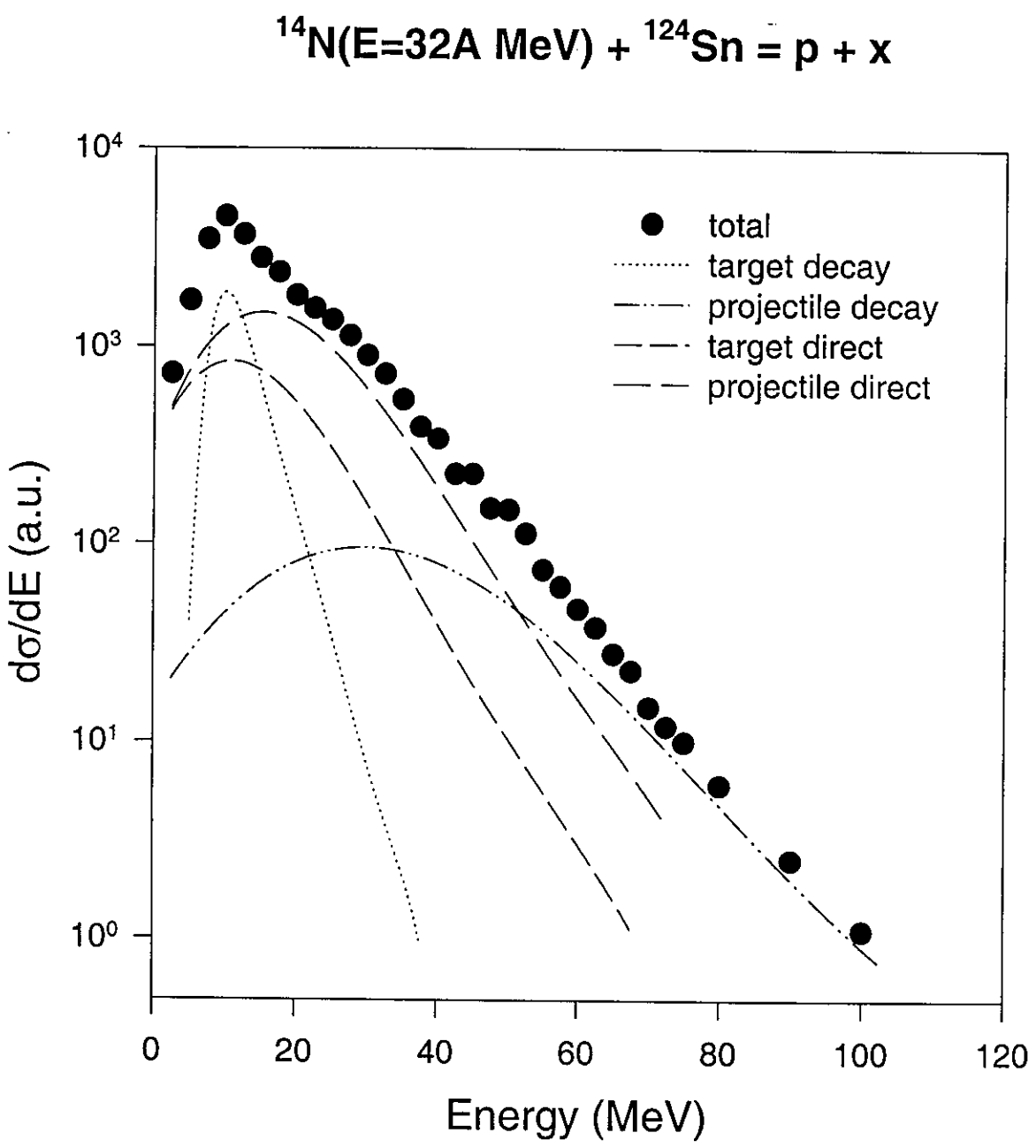
^{14}N(E=32A MeV) + ^{124}Sn = p + x
10^4
10^3
10^2
10^1
10^0
dσ/dE (a.u.)
0
20
40
60
80
100
120
Energy (MeV)
total
target decay
projectile decay
target direct
projectile direct

Fig. 11

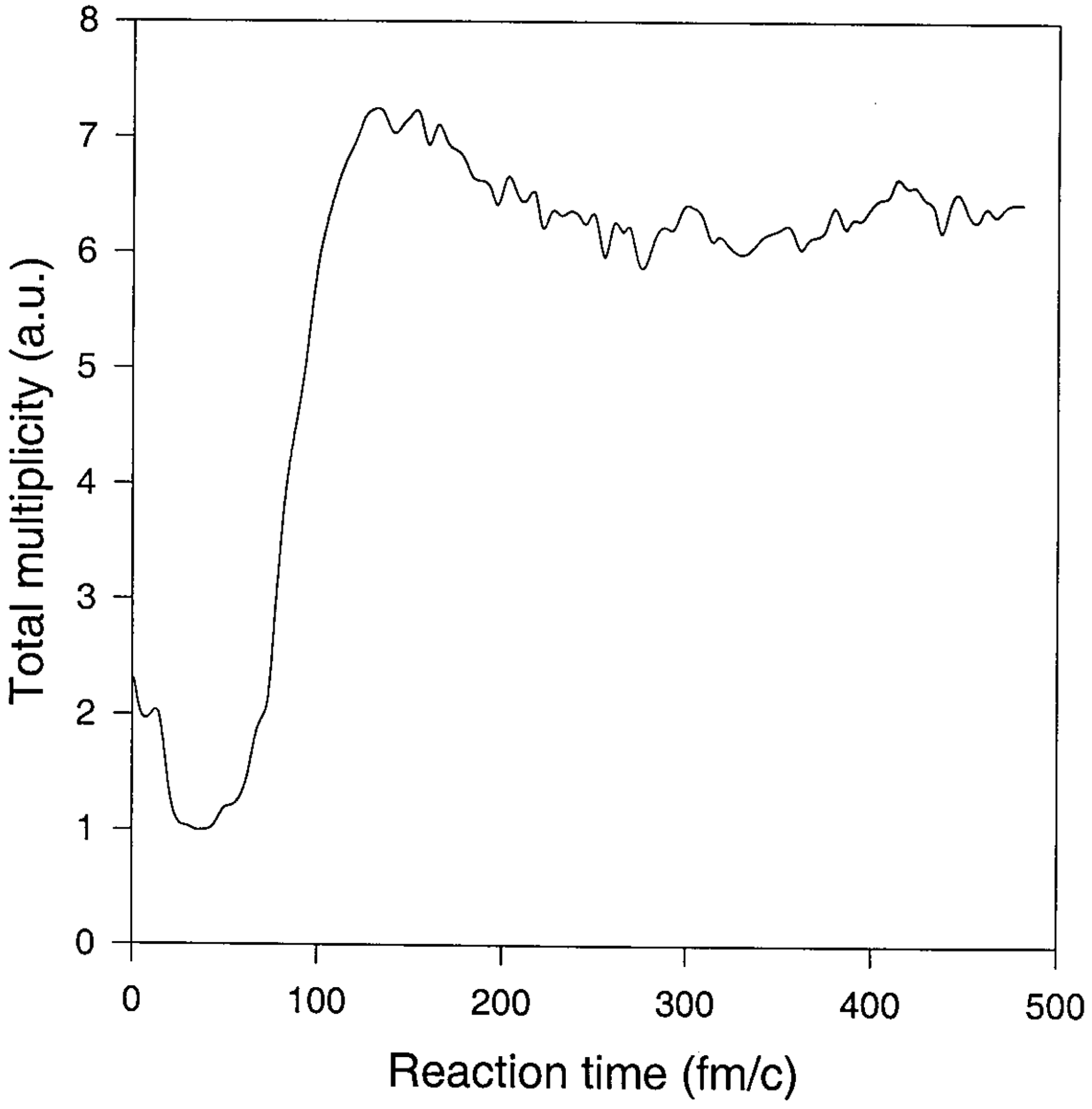
Total multiplicity (a.u.)
0
1
2
3
4
5
6
7
8
0
100
200
300
400
500
Reaction time (fm/c)

Fig. 12